Rotational Spectral Density Functions for Aqueous Sucrose: Experimental Determination Using ^{13}C NMR

Douglas C. McCain[†] and John L. Markley*[‡]

Contribution from the Department of Chemistry, University of Southern Mississippi, Hattiesburg, Mississippi 39406, and the Department of Biochemistry, University of Wisconsin—Madison, College of Agricultural and Life Sciences, Madison, Wisconsin 53706.
Received October 25, 1985

Abstract: ^{13}C NMR spin–lattice relaxation times and nuclear Overhauser enhancements were measured as a function of concentration, temperature, and magnetic field strength for sucrose solutions in D_2O. These data were used to determine the frequency dependence and amplitude of the rotational spectral density function, $J(\omega)$. We find that $J(\omega)$ has the same frequency dependence as the theoretical spectral density function for a rigid molecule, but it has a lower amplitude. At the average ring-carbon atom in sucrose, the low-frequency amplitude of $J(\omega)$ is about 89% of the theoretical rigid-molecule value. Presumably, the amplitude is lowered by rotational components of vibrational motions, which rapidly accomplish part of the averaging that otherwise would be performed by the slower molecular rotations of a rigid molecule. Our results also reveal small differences in the amplitudes of $J(\omega)$ at different sucrose ring positions; these differences can be used to measure the relative amplitudes of local torsional and vibrational motions.

NMR techniques frequently are used to measure molecular rotational correlation times. However, the method is indirect. Experimental nuclear spin relaxation times are proportional to the amplitudes of one or more spectral density functions that contain all the available information about molecular motions. Therefore, to derive correlation times from NMR data, one must know the spectral density functions.

For example, when a ^{13}C nucleus is relaxed by fluctuating dipolar fields from neighboring ^1H nuclei, its spin–lattice relaxation time, T_1, and nuclear Overhauser enhancement (NOE) factor, η, are given by[1,2]

$$T_1^{-1} = (1/10) \times (\hbar\gamma_H\gamma_C\Sigma_H\langle r_{CH}^{-3}\rangle)^2\{J(\omega_H - \omega_C) + 3J(\omega_C) + 6J(\omega_H + \omega_C)\} \quad (1)$$

$$\eta = \frac{(\gamma_H/\gamma_C)\{6J(\omega_H + \omega_C) - J(\omega_H - \omega_C)\}}{J(\omega_H - \omega_C) + 3J(\omega_C) + 6J(\omega_H + \omega_C)} \quad (2)$$

where $J(\omega)$ is a spectral density function, ω_H and ω_C are the precessional frequencies, and γ_H and γ_C are the gyromagnetic ratios of ^1H and ^{13}C, respectively.[3] The r_{CH} terms are C–H internuclear distances, and the summation runs over all hydrogen atoms in the molecule.

$J(\omega)$ is the Fourier transform of the correlation function[4-6]

$$J(\omega) = \int_0^\infty \langle A(0)A(t)\rangle(\cos \omega t)\, dt \quad (3)$$

where ω is an angular frequency and the term enclosed in brackets is the correlation function. $\langle A(0)A(t)\rangle$ describes the progressive loss of information as an evolving system decays from its initial state (at time $t = 0$); for use with eq 1, the correlation function is defined so that $\langle A^2(0)\rangle = 1.0$.

When the correlation function is a simple exponential decay

$$\langle A(0)A(t)\rangle = \langle A(0)^2\rangle \exp(-t/\tau_c) \quad (4)$$

$J(\omega)$ has the form

$$J(\omega) = \langle A(0)^2\rangle\tau_c/(1 + \omega^2\tau_c^2) \quad (5)$$

where τ_c is the correlation time. These equations are appropriate for many theoretical (and actual) physical systems. For example, eq 4 and 5 describe correctly the spectral density function for a rigid spherical molecule that rotates randomly in a viscous medium.[4-6]

Many other rotational spectral density functions have been proposed.[5] Some of these have been devised for special cases such as for small molecules in relatively nonviscous media, where correlation functions may decay nonexponentially. Others[7,8] describe the complex motions of nonspherical molecules for which more than one correlation time is required. We shall not be concerned here with such functions.

Recently, Levy, Karplus, and McCammon[4] have shown that the rigid-molecule assumption neglects important contributions from internal motion. Using molecular dynamics simulations, they demonstrated bimodal decay in the correlation functions for carbon atoms in proteins. A very rapid initial decay in $\langle A(0)A(t)\rangle$ is caused by angular components of internal motions (vibrations, torsional motions, etc.). However, internal motions alone are generally incapable of averaging an internuclear vector over all its possible orientations; therefore, the correlation function soon reaches a plateau value from which it slowly decays by overall molecular rotation with the usual molecular rotational correlation times. The important effect of rapid internal motion is to reduce the amplitude of $J(\omega)$ at NMR frequencies. Levy et al.[4] suggest that the function

$$J(\omega) = \langle A(0)A(p)\rangle\tau_c/(1 + \omega^2\tau_c^2) \quad (6)$$

is a good approximation at NMR frequencies. Here $\langle A(0)A(p)\rangle$ is the plateau amplitude at a time, p, when internal averaging is essentially complete but before rotational averaging has become significant (i.e., when $p \ll \tau_c$). Equation 6 reduces to eq 5 for a hypothetical, rigid molecule (where $p = 0$ because there is no vibrational averaging). For real molecules, the amplitude factor, $\langle A(0)A(p)\rangle$, has values between 1 and 0; as vibrational motions increase in importance, the amplitude factor decreases.

Other authors[9,10] have presented formulations similar to eq 6. For example, Lipari and Szabo[9] derived the spectral density function for a nonrigid molecule using the less restrictive assumption that the time-scale for internal motion is not neglegible

[†] University of Southern Mississippi.
[‡] University of Wisconsin—Madison.

(1) Abragam, A. *The Principles of Nuclear Magnetism*; Oxford University Press: London, 1961.
(2) Doddrell, D.; Glushko, V.; Allerhand, A. *J. Chem. Phys.* **1972**, *56*, 3683–3689.
(3) The constant terms are the following: $(\hbar\gamma_H\gamma_C)^2/10 = 3.602 \times 10^3$ nm^6 s^{-2} and $(\gamma_H/\gamma_C) = 3.977$.
(4) Levy, R. M.; Karplus, M.; McCammon, J. A. *J. Am. Chem. Soc.* **1981**, *103*, 994–996.
(5) Gordon, R. G. *Adv. Magn. Reson.* **1968**, *3*, 1–42.
(6) Boeré, R. T.; Kidd, R. G. *Annu. Rep. NMR Spectrosc.* **1982**, *13*, 319–385.
(7) Lambert, J. B.; Nienhuis, R. J.; Keepers, J. W. *Angew. Chem., Int. Ed. Engl.* **1981**, *20*, 487–500.
(8) Woessner, D. E. *J. Chem. Phys.* **1962**, *37*, 647–654.
(9) Lipari, G.; Szabo, A. *J. Am. Chem. Soc.* **1982**, *104*, 4546–4559.
(10) King, R.; Jardetzky, O. *Chem. Phys. Lett.* **1978**, *55*, 15–18.

0002-7863/86/1508-4259$01.50/0 © 1986 American Chemical Society

compared to that for molecular rotation. Their function

$$J(\omega) = S^2\tau_c/(1 + \omega^2\tau_c^2) + (1 - S^2)\tau_{eff} \quad (7)$$

includes the variables S, a generalized order parameter, and τ_{eff}, the effective correlation time for internal motion. In the limiting case of rapid internal motion ($\tau_{eff} \ll \tau_c$), eq 7 reduces to eq 6 with $S^2 = \langle A(0)A(p)\rangle$.

Our objective in this paper is to test eq 5, 6, and 7 experimentally. Our strategy is to determine the frequency dependence of $J(\omega)$ by varying ω (using different NMR spectrometers) and to measure the amplitude by comparing correlation times obtained independently with eq 1 and 2. The relaxation rate, $1/T_1$, is directly proportional to the amplitude of $J(\omega)$, whereas the nuclear Overhauser enhancement, η, is unaffected by a constant multiplication factor in $J(\omega)$ (e.g., by $\langle A(0)A(p)\rangle$) because it is proportional to a ratio of spectral density terms. Therefore, we can measure $\langle A(0)A(p)\rangle$ by adjusting its value to obtain simultaneously the same correlation times from both T_1 and NOE data.

The method we propose to use requires accurate experimental data from a molecule that has a known solution structure. Sucrose was chosen for this study because it occupies a single, nearly spherical conformation.[11,12] Also, strong solute–solvent interaction through hydrogen bonds ensures that rotation is controlled by viscous forces; therefore, we expect molecular rotational components of the correlation function to decay exponentially. Finally, because the rotational correlation times of sucrose ring-carbon atoms are nearly identical,[12] we can improve the experimental accuracy by averaging data.

A sucrose molecule has 12 carbon atoms, but for this analysis we are concerned only with the singly protonated ring-carbons that constitute a relatively rigid platform.[11,12] The ^{13}C spectrum of sucrose has been assigned,[11] and the eight ring-carbons are identified with peaks 2–9 (numbered consecutively from low field). Other peaks are assigned to ring-carbons not bonded to hydrogen (peak 1) or to carbons in hydroxymethyl groups (peaks 10–12).

Experimental Section

Solutions were prepared from reagent grade sucrose and D_2O (Bio-Rad, 99.8% D). Samples at five sucrose concentrations (1.0, 0.50, 0.25, 0.10, and 0.010 M) were deoxygenated by N_2 bubbling and sealed in glass NMR sample tubes. Samples stored at 4 °C showed no measurable change in T_1 or η during 1 y of repeated use.

To study the effects of varying magnetic field strength, we used four different NMR spectrometers: Nicolet Models NT-150, NT-200, NT-360, and NT-470 operating at ^{13}C frequencies of 37.74, 50.31, 90.54, and 118.21 MHz with proton decoupling at 150, 200, 360, and 470 MHz, respectively. Probes accepting 8-mm sample tubes were used on the NT-360 and NT-470; the NT-150 and NT-200 used 12-mm samples. Sample temperatures were controlled to an accuracy of +/−2 °C.

Power levels for square-wave-modulated proton decoupling were chosen to be just sufficient to collapse the C–H coupling with a minimum of radiofrequency heating. Decoupler power levels at 150 and 200 MHz produced a negligible temperature rise (less than 1 °C). More radio frequency power was required at 360 and 470 MHz, causing minor heating; experimental temperatures at these fields were corrected (up to 2 °C) by using estimated correction factors. The transmitter frequency was set near the center of the sucrose spectrum (ca. 76 ppm downfield from Me_4Si), and the 180° pulse width was redetermined within +/−5 deg for each sample or temperature change. We used 8K data points and a spectral window covering 35–40 ppm.

T_1 measurements used the inversion–recovery pulse sequence (180°–τ–90°–AT–PD) where AT represents the signal acquisition time and PD is a pulse delay (AT + PD $\simeq 5T_1$). From 10 to 32 (usually 14) variable delay (τ) values were used for each experimental run; they were chosen to be spaced in logarithmic increments of time from less than $0.1T_1$ to ca. $5T_1$ and called in random order. The time required to obtain each data set varied from 5 to 10 min for 1.0 M to 10 h for 0.010 M samples.

Free induction decays were apodized by using exponential line-broadening parameters approximately equal to the unapodized line widths, which varied with temperature and concentration. After Fourier transformation, T_1 was determined by a subroutine (supplied with the Nicolet software) that fits a parabolic function to those data points near the top of a selected spectral peak to find corrected peak heights, $S(\tau)$. These data were then fitted to the equation[13]

$$S(\tau) = S(\infty)\{1 - (1 + W(1 - \exp(-(AT + PD)/T_1))\exp(-\tau/T_1))\} \quad (8)$$

to obtain T_1, W, and $S(\infty)$. The W term partially corrects for errors caused by inhomogeneous radio frequency fields. W is primarily a function of probe geometry; each spectrometer has its own characteristic value in the range from 0.7 to 0.95. All our data fit eq 8 well; we found no evidence of nonexponential recovery.

The standard gated decoupling technique[14] was used to measure η. The decoupler was square-wave modulated at 150 Hz and set to the minimum level at which the measured enhancement was independent of radio frequency power. Recycle times were approximately $10T_1$.

On the basis of internal consistencies within our data,[12] we estimated the precision of an individual T_1 measurement to be better than +/−10% for the three most concentrated solutions, +/−15% for 0.10 M, and +/−20% for 0.010 M. Measured Overhauser enhancements were not as precise as T_1 data (error limits ca. 50% greater). By using averages from eight NMR lines, the error limits were reduced considerably (by a factor of $\sqrt{8}$) from those of individual measurements. Temperature uncertainties (+/−2 °C) also were a major source of error.

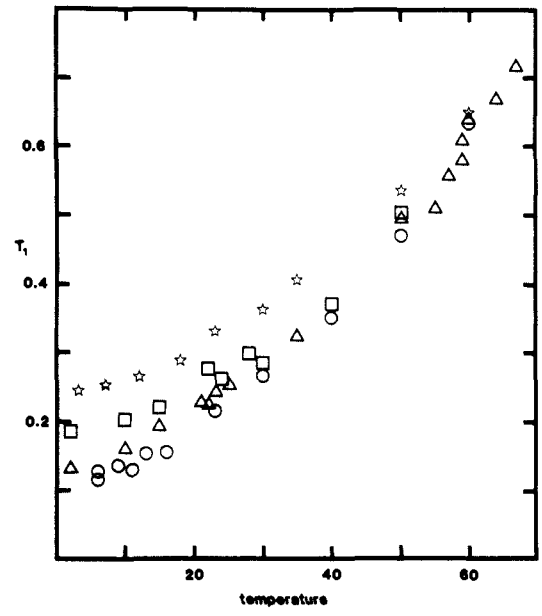

Figure 1. Experimental ^{13}C nuclear spin–lattice relaxation times, T_1 (in s) vs. temperatures (in °C) for 1.0 M sucrose in D_2O. To reduce scatter, each point was obtained by averaging T_1 values measured independently from each of eight ring-carbon atoms. NMR spectrometers operating at four different magnetic fields were used; the circles, triangles, squares, and stars represent data obtained on spectrometers with ^1H NMR frequencies of 150, 200, 360, and 470 MHz., respectively. Note that relaxation times are somewhat field dependent, especially at low temperatures.

Results and Discussion

Figures 1 and 2 illustrate the field and temperature dependence of T_1 and η for 1.0 M sucrose in D_2O. Each point represents the average of eight individual measurements (from each of the eight singly protonated ring-carbon atoms) made during a single experimental run at one of four different magnetic field strengths (i.e., on one of four different NMR spectrometers). T_1 and η are field dependent at low temperatures where τ_c is long. As temperature increases, η approaches its theoretical limiting value of 1.988 which is reached when $\omega^2\tau_c^2 \ll 1$. Similar results (not shown) were obtained at lower sucrose concentrations. Since correlation times are shorter at low concentrations, the data points for T_1 and η were displaced upward relative to the points in Figures 1 and 2, and the field dependence was reduced.

In order to derive accurate correlation times from relaxation data, using eq 1, we require an accurate value for $\Sigma_H\langle r_{CH}^{-3}\rangle^2$. For ring-carbon atoms in sucrose, the apparent C–H bond length

(11) Bock, K.; Lemieux, R. U. *Carbohydr. Res.* **1982**, *100*, 63–74.
(12) McCain, D. C.; Markley, J. L. *Carbohydr. Res.*, in press.
(13) Levy, G. C.; Peat, I. R. *J. Magn. Reson.* **1975**, *18*, 500–521.
(14) Canet, D. *J. Magn. Reson.* **1976**, *23*, 361–364.

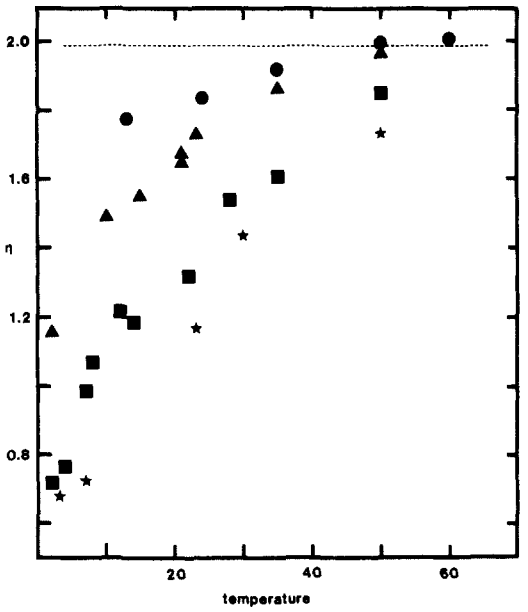

Figure 2. Experimental ^{13}C nuclear Overhauser enhancements, η, vs. temperature (in °C) for 1.0 M sucrose in D_2O. Each point represents the average enhancement from eight ring-carbon atoms. The circles, triangles, squares, and stars are from data obtained at ^1H NMR frequencies of 150, 200, 360, and 470 MHz, respectively. The dashed line (at $\eta = 1.988$) corresponds to the theoretical maximum enhancement (for pure ^{13}C–^1H dipole–dipole relaxation) that is approached when correlation times are very short. Note that experimental data approach the theoretical limiting value at high temperatures and that enhancements are strongly field dependent at low temperatures.

(i.e., the distance between maxima on a density distribution plot) is 0.11016 +/- 0.00025 nm, as measured by neutron diffraction.[15] This is a much more accurate bond length than could be obtained by X-ray methods; however, certain corrections are necessary. The effective bond length is influenced by vibrational motion and is not the same as the apparent bond length.[16,17] Brown and Levy[15] estimated a mean length of 0.1110 nm from their neutron diffraction data. By using the mean length in place of the apparent length, we correct for the influence of bending vibrational modes on r_{CH} without correcting for their effect on the rotational correlation function. An additional correction is necessary because the expectation value, $\langle r_{CH}^{-3}\rangle^2$, is not exactly equal to r_{CH}^{-6}; Henry and Szabo[18] showed that this correction (based on the combined effect of harmonic and anharmonic C–H stretching force constants) increases the effective value of r_{CH} by about 1%, i.e., to 0.112 nm. Using this value, we obtain $\langle r_{CH}^{-3}\rangle^2 = 5.04 \times 10^5$ nm^{-6} as our best estimate for the contribution from directly bonded hydrogen atoms.[19]

The contribution from distant protons (those not directly bonded to the reference carbon) also must be considered. By using crystal structure data,[15] and including all the hydrogen atoms in sucrose except those in hydroxyl groups (which will exchange with D_2O), we calculate an extra contribution to $\Sigma_H\langle r_{CH}^{-3}\rangle^2$ of 0.26×10^5 nm^{-6} from the net effect of distant hydrogens as experienced by the average ring-carbon atom. We shall neglect mean length and zero-point corrections for the distant hydrogens as well as other factors (such as cross correlation) that may influence relaxation rates because these effects are insignificant compared to terms already calculated; therefore, our best estimate for the total $\Sigma_H\langle r_{CH}^{-3}\rangle^2$ at the average ring-carbon atom is 5.30×10^5 nm^{-6}.

It is difficult to estimate error limits for $\Sigma_H\langle r_{CH}^{-3}\rangle^2$; the corrections we have made are quite significant, but they are only approximations. We believe our value is accurate to within +/-5%.[20]

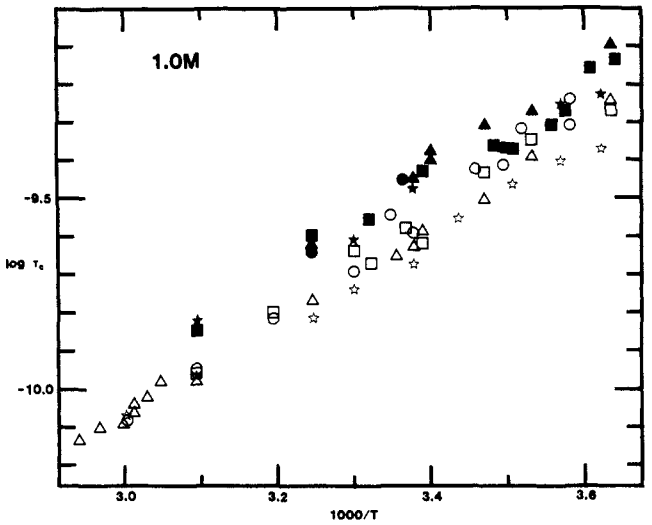

Figure 3. A plot of log τ_c (with τ_c in s) vs. $1000/T$ (K^{-1}). The points were obtained by solving eq 1, 2, and 5 for τ_c, using the experimental T_1 and NOE data displayed in Figures 1 and 2. Symbols have the same meanings as in Figures 1 and 2; open symbols represent correlation times derived from T_1 data while closed symbols were obtained from NOE measurements.

A sucrose molecule is not perfectly spherical; in solution it rotates anisotropically. Anisotropic rotation is described by a spectral density function featuring two or three different rotational correlation times. However, we believe that a function with a single τ_c is sufficient for our analysis. To support our use of this simplification, we offer the following arguments: (1) The rotational motions of sucrose are only slightly anisotropic, and the correlation times are almost equal to each other.[11,12] In the limiting case when anisotropic rotational correlation times become equal, the spectral density becomes a function of a single τ_c. (2) In order to improve the precision of the measurements, we have averaged data from eight ring-carbon atoms. The average motion of eight differently oriented C–H bond vectors is more nearly isotropic than is the motion of a single vector.

Figure 3 presents a test of eq 5, the spectral density function for a rigid molecule. Correlation times were calculated from the experimental 1.0 M sucrose data displayed in Figures 1 and 2 by using eq 1, 2, and 5 and with $\Sigma\langle r_{CH}^{-3}\rangle^2 = 5.30 \times 10^5$ nm^{-6}. Nuclear Overhauser enhancements near the theoretical limit (the dashed line in Figure 2) were not used because they produced very uncertain values of τ_c.

Figure 3 demonstrates a discrepancy between rotational correlation times derived separately from T_1 and NOE data with eq 5. We cannot remove the discrepancy by postulating additional relaxation mechanisms (i.e., mechanims not involving dipole–dipole interaction), because another parallel mechanism would decrease both η and T_1 in such a way as to increase the calculated correlation times in both sets of data. The discrepancy could be caused by an error of 11% in the value of $\Sigma_H\langle r_{CH}^{-3}\rangle^2$; however, we belive that the corrections described above have reduced the probable range of error to less than 5%. The fact that T_1 and NOE data form nearly parallel lines indicates that the discrepancy involves a multiplication factor in eq 5 that is independent of both temperature and τ_c.

Figure 4 was prepared from the same experimental data as used for Figure 3, but the calculations used eq 6. A simultaneous, least-squares fit to both the T_1 and the NOE data was used to set the value of the amplitude factor, $\langle A(0)A(p)\rangle$, to 0.89. Figure 4 demonstrates that the discrepancy in Figure 3 can be eliminated

(15) Brown, G. M.; Levy, H. A. *Acta Crystallogr.* **1973**, *B29*, 790–797.
(16) Busing, W. R.; Levy, H. A. *Acta Crystallogr.* **1964**, *17*, 142–146.
(17) Dill, K.; Allerhand, A. *J. Am. Chem. Soc.* **1979**, *101*, 4376–4378.
(18) Henry, E. R.; Szabo, A. *J. Chem. Phys.* **1985** *82*, 4753–4761.
(19) The vibrational corrections could have been included in the vibrational averaging term $\langle A(0)A(p)\rangle$. We chose to incorporate them into $\Sigma_H\langle r_{CH}^{-3}\rangle^2$ in order to restrict $\langle A(0)A(p)\rangle$ to purely orientational effects.
(20) If a better estimate becomes available it will be a simple matter to adjust our reported values of $\langle A(0)A(p)\rangle$ because our experiments measure the product $\sum_H\langle r_{CH}^{-3}\rangle^2\langle A(0)A(p)\rangle$ rather than directly measuring the amplitude of $J(\omega)$.

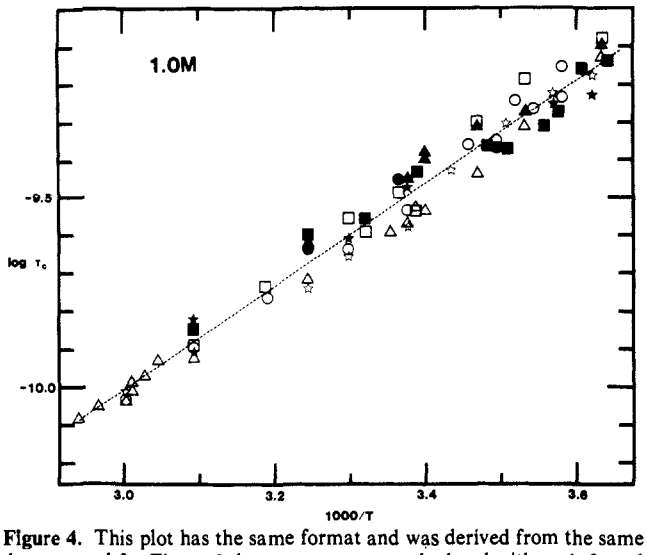

Figure 4. This plot has the same format and was derived from the same data as used for Figure 3; however, τ_c was recalculated with eq 1, 2, and 6 with $\langle A(0)A(p)\rangle = 0.89$. Symbols have the same meanings as in Figures 1, 2, and 3. The dashed line is a linear least-squares fit to all the data. Note that correlation times derived from T_1 and η coincide within experimental error. Points that represent NOE data are unchanged from Figure 3 because correlation times derived from eq 2 are independent of $\langle A(0)A(p)\rangle$, while points for T_1 data, derived from eq 1, are displaced upward.

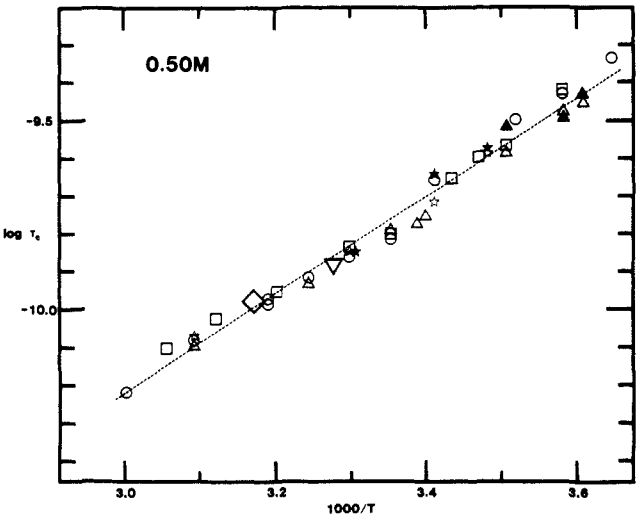

Figure 5. log τ_c vs. $1000/T$ for 0.50 M sucrose in D_2O. The correlation times were calculated from eq 1, 2, and 6 with $\langle A(0)A(p)\rangle = 0.89$. Symbols have the same meaning as in Figures 3 and 4; open symbols represent correlation times derived from T_1 data; closed symbols are for NOE data. The two additional symbols, the large diamond and the large inverted triangle, represent T_1 data from the literature (see text for discussion); all other data are from this work.

by using a correlation function with two independent variables. Random experimental scatter probably contributes error limits of +/−2% for the amplitude factor; however, correlation times measured from T_1 data with eq 1 cannot be more accurate than the value of $\Sigma_H\langle r_{CH}^{-3}\rangle^2$; therefore, we estimate error limits of ca. +/−5% for $\langle A(0)A(p)\rangle$.[20]

Figure 4 also shows that eq 6 simultaneously fits the data from four different field strengths. When the τ_{eff} term becomes significant, eq 7 has a different field dependence than eq 6; otherwise, the two equations are experimentally indistinguishable. Therefore, we conclude that within our limits of experimental error the approximation $\tau_{eff} \ll \tau_c$ is a good one and that eq 7, with its additional adjustable parameter, is unnecessary. In aqueous sucrose, τ_{eff} would have to reach values in excess of 20 ps before eq 6 and 7 would differ significantly. Molecular dynamics simulations suggest that τ_{eff} is about 2 ps in proteins.[4] We suppose

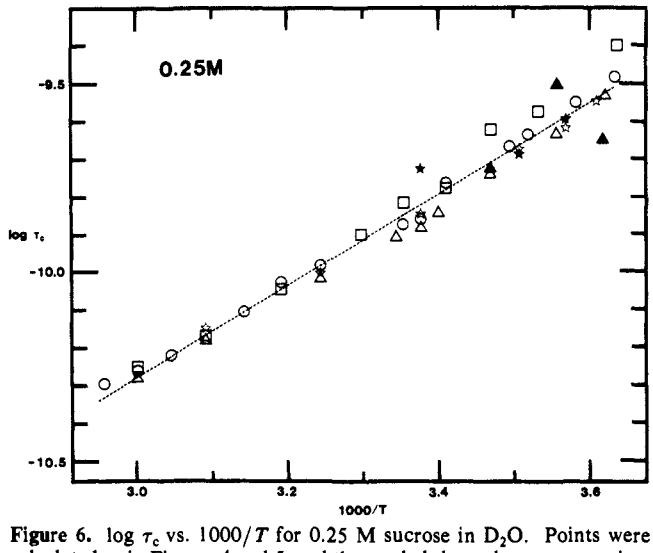

Figure 6. log τ_c vs. $1000/T$ for 0.25 M sucrose in D_2O. Points were calculated as in Figures 4 and 5, and the symbols have the same meaning.

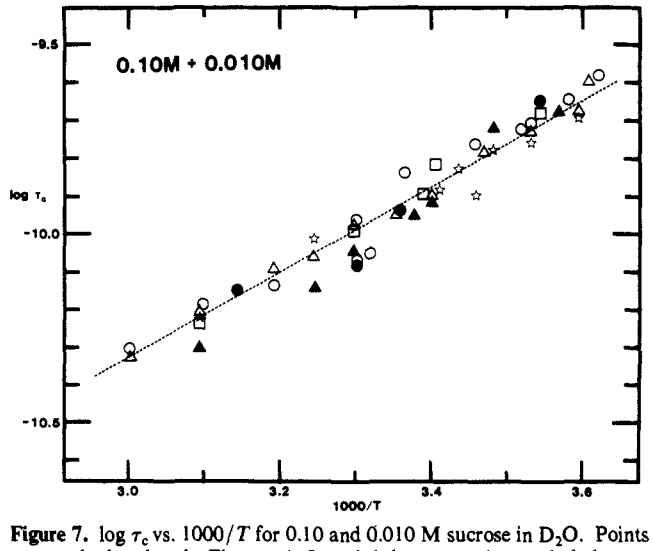

Figure 7. log τ_c vs. $1000/T$ for 0.10 and 0.010 M sucrose in D_2O. Points were calculated as in Figures 4, 5, and 6; however, the symbols have a different meaning: open symbols represent T_1 data obtained from 0.10 M solutions while closed symbols are for T_1 data from 0.010 M sucrose. No NOE data are shown. As in all the other figures, circles, triangles, squares, and stars are used to signify data from spectrometers with ^1H NMR frequencies of 150, 200, 360, and 470 MHz, respectively.

this value is the correct order of magnitude for sucrose as well.

Figures 5–7 display correlation times calculated with use of data from lower sucrose concentrations. We used eq 6 and the same amplitude factor as in Figure 4, $\langle A(0)A(p)\rangle = 0.89$. Data obtained at lower concentrations are less appropriate for measuring the amplitude factor because as correlation times become shorter, η approaches its limiting value of 1.988, and the correlation times derived from NOE data become much less accurate. This is why we show fewer NOE points in Figures 5 and 6 and none at all in Figure 7 and why we show NOE data only at the lower temperatures where correlation times are relatively long. Despite the limited number of NOE data points, it is apparent that the amplitude factor determined with data from 1.0 M sucrose is correct within experimental error at lower concentrations.

Figure 5 includes two data points extracted from the literature which show that our measurements are in good agreement with previously reported results. The diamond-shaped symbol represents a measurement by Allerhand et al.[21] whose results from 0.5 M sucrose in D_2O at 42 °C average to $T_1 = 0.56$ s for peaks 2–9.

(21) Allerhand, A.; Doddrell, D.; Komoroski, R. *J. Chem. Phys.* **1971**, *55*, 189–198.

Bock and Lemieux[11] also studied 0.5 M sucrose in D_2O; the large inverted triangle represents their average T_1 of 0.47 s at 32 °C.

The slopes of the curves in Figures 4–7 can be used to measure E^*, the activation energy for molecular rotation. The slope of $(\Delta \ln \tau_c/\Delta(1/T))$ is equal to E^*/R where $R = 8.31$ J/(mol K). By using the least-squares fits indicated by dashed lines (in Figures 4–7), we calculated activation energies of 26.3, 24.9, 23.2, and 21.9 kJ/mol at sucrose concentrations of 1.0, 0.50, 0.25, and 0.10 M, respectively. The data at 0.010 M are not accurate enough for comparison. These data extrapolate to a value of 21.9 +/- 0.3 kJ/mol at infinite dilution. Rotational correlation times for Brownian diffusion in a viscous medium are proportional, theoretically,[6] to the ratio of solvent viscosity to temperature. For D_2O at 20 °C this corresponds to a theoretical activation energy of[22] 22 kJ/mol, in excellent agreement with our data.

We may also use the least-squares fits to determine accurate rotational correlation times at specific temperatures, although it must be remembered that τ_c is approximately the average of several anisotropic correlation times. At 20 °C we find correlation times of 0.357, 0.205, 0.166, and 0.138 ns at concentrations of 1.0, 0.50, 0.25, and 0.10 M, respectively. These data extrapolate to a limiting correlation time of 0.131 ns at infinite dilution, corresponding to the Stokes rotational correlation time (in a medium with the same viscosity as D_2O) of a sphere with diameter equal to 0.93 nm and a volume of 0.42 nm^3. The volume of a sucrose molecule, computed from its crystal density, is 0.36 nm^3; the slightly larger experimental solution volume may be caused by solvation.

To determine the average amplitude factor, $\langle A(0)A(p)\rangle$, as described above, we first averaged experimental T_1 and NOE data from the eight ring-carbon atoms; this was done to reduce experimental scatter. We would have preferred to calculate individual amplitude factors for each of the ring-carbon atoms; indeed, such calculations were attempted with the same method, but with individual T_1 and NOE measurements in place of the averages. Our calculated amplitudes at the different ring positions differed from the average amplitude ($\langle A(0)A(p)\rangle = 0.89$) by an average deviation of about 4%. However, a statistical analysis of the data suggested that experimental errors should contribute random scatter at a level of about 4% and therefore that experimental amplitudes from different ring positions could not be reliably distinguished from each other.

Having failed to calculate individual amplitude factors with the direct method, we tried another approach. We normalized the data and calculated relative amplitude factors. Normalization involves a different kind of averaging than does the direct method; it allows us simultaneously to use data from all temperatures, fields, and concentrations and thereby to reduce experimental scatter. In addition, it effectively suppresses systematic errors that affect equally all peaks in the NMR spectrum. For example, normalization cancels errors such as those caused by inaccurate sample temperatures or insufficient decoupler power. The major disadvantage of the normalization method is that it measures relative amplitude factors instead of absolute values. However, in combination with the average amplitude factor already determined, we were able to reconstruct the absolute values.

To normalize, we took the data from each experimental run (eight T_1 or η values) and calculated eight τ_c values using eq 2 and 6 (for NOE data) or eq 1 and 6 with $\langle A(0)A(p)\rangle = 0.89$ (for T_1 data).[23] Normalized correlation times were obtained by dividing individual correlation times by the average correlation time from all eight peaks as measured in the same experiment. We found no evidence of temperature, concentration, or field dependence in our normalized data. Assuming that all such dependence indeed has been removed, the averaged data from each ring-carbon provides accurate, relative correlation times.[24] The averaged, normalized correlation times derived from NOE data, $\tau_c(\eta)$, are directly proportional to the actual rotational correlation times and are slightly different at each ring-carbon because of anisotropic motion. Averages derived from T_1 data, $\tau_c(T_1)$, are proportional to the product of τ_c and $\langle A(0)A(p)\rangle$ (even though the raw data were analyzed assuming $\langle A(0)A(p)\rangle = 0.89$); therefore, the ratio $\tau_c(T_1)/\tau_c(\eta)$ is proportional to $\langle A(0)A(p)\rangle$.

Table I displays $\tau_c(\eta)$ and $\tau_c(T_1)$ and the calculated value of $\langle A(0)A(p)\rangle$.[25] The averages were obtained from 41 NOE data sets (the same ones as used for NOE data in Figures 4–6) and 97 T_1 data sets. T_1 data sets were used only when $\omega_H\tau_c < 0.4$, because at longer correlation times the shape of the spectral density function causes T_1 to become insensitive to τ_c. As a result of these

Table I. Normalized Correlation Times and Spectral Density Amplitude Factors for the Ring Carbons of Sucrose

peak[a]	assign[b]	$\tau_c(\eta)$[c]	$\tau_c(T_1)$[d]	$\langle A(0)A(p)\rangle$[e]
2	1^g	0.975	1.053	0.962
3	5^f	1.005	1.047	0.928
4	3^f	1.050	1.050	0.891
5	4^f	1.021	0.994	0.867
6	3^g	1.010	0.956	0.843
7	5^g	0.970	0.958	0.880
8	2^g	0.976	0.984	0.898
9	4^g	0.994	0.960	0.861

[a] Peaks are numbered consecutively as they appear in the spectrum, from low to high field. Data from peaks 1, 10, 11, and 12 are not used. [b] Peak assignments from the following: Bock, K.; Lemieux, R. U. *Carbohyd. Res.* **1982**, *100*, 63–74. Carbon atoms are numbered according to the conventional system for sucrose; superscripts g and f refer to glucose and fructose carbons, respectively. [c] Measured by using eq 2 and 6 with 41 different NOE data sets. Normalized to an average value of 1.0. Error limits are +/-0.017 for one standard deviation of the mean (SDM). Since these correlation times are normalized, they are unitless. [d] Measured by using eq 1 and 6 with 97 different T_1 data sets. Normalized to average 1.0. Error limits (one SDM) are +/-0.007. [e] Calculated from $\langle A(0)A(p)\rangle = 0.891\tau_c(T_1)/\tau_c(\eta)$. Relative amplitude factors (comparing one ring-carbon to another) are known more accurately (to ca. +/-2%) than absolute amplitudes, which are subject to additional errors of +/-5%.

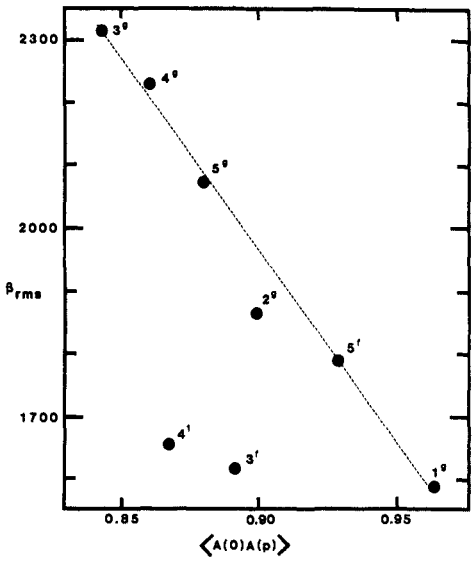

Figure 8. This plot shows the correlation between spectral density amplitude factors, $\langle A(0)A(p)\rangle$ (from Table I), and thermal amplitudes, β_{rms}, calculated from the sucrose crystal structure data of G. M. Brown and H. A. Levy.[15] Each point is labeled with its ring-carbon assignment as defined in Table I.

(22) Kirshenbaum, I. *Physical Properties and Analysis of Heavy Water*; McGraw-Hill: New York, 1951.

(23) The contribution to $\Sigma_H(r_{CH}^{-3})^2$ from distant (not directly bonded) hydrogen atoms is not the same at different ring-carbon positions. We used 5.17×10^5 at carbons 1^g and 3^f, 5.43×10^5 at carbons 5^g and 5^f, and 5.30×10^5 nm^{-6} at all other carbons.

(24) Error limits for the average normalized values can be estimated from their standard deviations. The standard deviation of the mean (SDM) is the standard deviation divided by the square root of the number of experimental data points. At the 95% confidence level, the true value lies within +/-2 SDM of the experimental average.

(25) Ratios were multiplied by the average amplitude factor, 0.89, to recover absolute amplitudes from the normalized data.

restrictions, most of the NOE data came from the two higher field strengths (^{1}H NMR frequencies of 360 and 470 MHz) and most of the T_1 data came from the lower fields (150 and 200 MHz).

Table I demonstrates that normalized correlation times do not differ much from unity, but the differences are highly significant (much greater than +/-2 SDM).[24] All values should be 1.000 (within experimental error) if correlation times and amplitude factors were identical at each ring-carbon position. The table also shows that amplitude factors differ significantly with ring position. The greatest difference in $\langle A(0)A(p)\rangle$ (between carbons 1^g and 3^g) is greater than 6 SDM.

Differences among the amplitude factors are related to flexibility in the molecular structure. The largest amplitude factor (indicating the most restricted vibrational motion) is found at a bridgehead carbon (1^g), and the smallest (i.e., the least restricted motion) is found at the only ring-carbon (3^g) that is separated by two C-C bonds from either a bridgehead or a bulky hydroxymethyl group.

Our data in Table I describe the relative vibrational amplitudes at each of the ring-carbon atoms. Vibrational amplitudes also can be measured in crystallographic diffraction studies. Brown and Levy[15] report thermal amplitudes from a neutron diffraction study of sucrose. Using their data (Table 3 in ref 15), we have calculated a parameter, β_{rms}, which is the square root of the sum of the squares of the thermal factors (β_{11}, β_{22}, and β_{33}) for each ring-carbon atom and for the hydrogen atom bonded directly to it.

Figure 8 shows a plot of $\langle A(0)A(p)\rangle$ vs. β_{rms}. If vibrational motions in the crystal were identical with those in solution, one would expect good correlation between both data sets; indeed, one would expect all points to lie on a smooth curve with a negative slope such as the one suggested by the straight line. Two deviant points (3^f and 4^f) lie well below the others, suggesting that vibrational amplitudes at these two carbons are greater in solution than in the crystal.

Bock and Lemieux[11] studied aqueous sucrose using NMR as well as molecular modeling calculations. They concluded that the conformation of aqueous sucrose is similar to that of the crystal; the major difference in solution is the loss of one intramolecular hydrogen bond which causes increased flexibility in the fructose ring. Our data support their conclusion and show that the increased flexibility is located almost entirely at carbons 3^f and 4^f.

Acknowledgment. The authors thank Dr. C. B. Post for helpful discussions. This research was supported in part by the National Institutes of Health, Division of Research Resources (Grants RR01077 and RR02301). The work was carried out in the Purdue University Biological Magnetic Resonance Laboratory.

Registry No. Sucrose, 57-50-1.

An Analysis of Non-Lorentzian ^{23}Na Line Shapes in Two Model Systems

Laura Lerner and Dennis A. Torchia*

Contribution from the Bone Research Branch, National Institute of Dental Research, National Institutes of Health, Bethesda, Maryland 20892. *Received October 17, 1985*

Abstract: In view of the increasing interest in applications of ^{23}Na NMR to biochemical and biological research, we have investigated the causes of non-Lorentzian ^{23}Na line shapes in two model systems: (a) sodium chloride in an aqueous suspension of sodium laurate; and (b) sodium chloride in glycerin. Analysis of the field and temperature dependence of T_1, T_2, and line shapes leads us to conclude that the non-Lorentzian line shape observed in sodium laurate results from rapid exchange of a small fraction of sodium ions in the slow motion limit with sodium ions in the extreme narrowing region. In contrast, the non-Lorentzian line shape of sodium in glycerin arises from a single population of ions in the slow motion region. In this case, an approximate value of the ^{23}Na quadrupole coupling constant, 1.6 MHz, is derived from the temperature-dependent relaxation data.

Nuclear magnetic resonance spectroscopy (NMR) of quadrupolar nuclei has been used to assess binding of cations to macromolecules such as DNA[1], calmodulin[2], and proteoglycans[3]. Binding of a cation containing a quadrupolar nucleus to a macromolecule is made manifest by the changes in line shape and line width that occur when association with a macromolecule (typical correlation time 10^{-9} s) increases the correlation time of the cation (typical correlation time 10^{-12} s). Binding may also change the electric field gradient at the nucleus.

Non-Lorentzian line shapes have been reported frequently in NMR studies[1,4] of cations having $I \geq 1$ in solutions of macromolecules and in intact tissue. It is therefore important to determine the sources of non-Lorentzian line shapes for these nuclei.

The NMR line shape and relaxation rates of quadrupolar nuclei depend on the value of the product of the Larmor frequency, ω_0, and the rotational correlation time, τ_c. If $(\omega_0\tau_c)^2$ is much less than 1 (extreme narrowing region), then the line shape is Lorentzian and $T_1 = T_2$. T_1 and T_2 are independent of ω_0, and they decrease as τ_c increases.[5] When $(\omega_0\tau_c)^2$ is approximately equal to 1, T_1 is at its minimum. (Actually, relaxation outside the extreme narrowing region is characterized by more than one relaxation time, as described below.)

If $(\omega_0\tau_c)^2$ is greater than 1 (slow motion region), the line shape is non-Lorentzian, and the decays of the longitudinal and transverse magnetizations are described by the sums of exponentials.[6] For nuclei with $I = {}^3/_2$ (for example, ^{23}Na), the line shape consists of two components: 60% of the signal intensity characterized by

(1) Nordenskiold, L.; Chang, D. K.; Anderson, C. F.; Record, M. T., Jr. *Biochemistry* **1984**, *23*, 4309-4317.
(2) Andersson, T.; Drakenberg, T.; Forsen, S.; Thulin, E. *Eur. J. Biochem.* **1982**, *126*, 501-505.
(3) Lerner, L.; Torchia, D. A. *J. Biol. Chem.*, in press.
(4) (a) Berendsen, H. J. C.; Edzes, H. T. *Ann. N.Y. Acad. Sci.* **1973**, *204*, 459-485. (b) Lindman, B. In *NMR of Newly Accessible Nuclei*; Laszlo, P., Ed.; Academic: New York, 1983; 1, pp 193-231. (c) Detellier, C. In *NMR of Newly Accessible Nuclei*; Laszlo, P., Ed.; Academic: New York, 1983; Vol. 2, pp 105-151. (d) Lerner, L.; Torchia, D. A., manuscript in preparation.
(5) Abragam, A. *The Principles of Nuclear Magnetism*; Clarendon Press: Oxford, 1961.
(6) Hubbard, P. S. *J. Chem. Phys.* **1970**, *53*, 985-987.

This article not subject to U.S. Copyright. Published 1986 by the American Chemical Society